CardioVascular and Interventional Radiology

Cardiovasc Intervent Radiol (1999) 22:1–6

CLINICAL INVESTIGATIONS

Detection of Accessory Renal Arteries with Virtual Vascular Endoscopy of the Aorta

Emanuele Neri, Davide Caramella, Cristina Bisogni, Edoardo Laiolo, Francesco Trincavelli, Adriano Viviani, Claudio Vignali, Roberto Cioni, Carlo Bartolozzi

Diagnostic and Interventional Radiology, Department of Oncology, University of Pisa, Via Roma 67, I-56100 Pisa, Italy

Abstract

Purpose: To evaluate the diagnostic accuracy of virtual vascular endoscopy (VVE) in the detection of accessory renal arteries.

Methods: We retrospectively reviewed the CT angiography data sets of 67 patients (29 male and 38 female; age range 17–72 years, mean age 53 years) imaged for the study of the renal arteries, and affected by renovascular hypertension. All patients also had intraarterial digital subtraction angiography (DSA). CT angiography data sets were processed to obtain maximum intensity projection (MIP) and surface-rendered VVE of the aorta. Axial images, MIP, and VVE were evaluated separately and in combination in the detection of accessory renal arteries. Their results in terms of sensitivity and specificity were then compared with DSA.

Results: Axial images had a sensitivity of 88% and specificity of 94% for accessory renal artery detection, MIP had a sensitivity of 88% and specificity of 98%, and VVE had a sensitivity of 63% and a specificity of 88% ($p < 0.05$ vs DSA), but these increased to 88% and 98% respectively if endoscopic views were integrated with the other display techniques.

Conclusion: VVE based on surface rendering does not add substantial benefits to CTY angiography; by contrast MIP is the most accurate display technique for the detection of accessory renal arteries.

Key words: Images, virtual—Computed tomography, helical—Renal arteries—Arteries, abnormalities

Accessory renal arteries are common, being found in 20%–30% of individuals, and are regarded as persistent embryonic lateral splanchnic arteries arising above or below the main renal artery. Rarely they arise from the celiac, splenic, or mesenteric arteries, near the aortic bifurcation, or from the common iliac arteries [1–4]. In a recent anatomic study of 140 human fetuses [5], accessory renal arteries were observed in 21.1% of cases, as a single (19.2%), double (2.1%), or triple artery (0.7%).

Correct evaluation of these additional branches is necessary in situations that require an accurate depiction of renal arterial anatomy. These situations include renal transplantation (in which all accessory renal arteries and the main artery of the donor must be reimplanted to prevent parenchymal ischemia), surgical reconstruction of the abdominal aorta (to avoid ligation of accessory renal arteries) and renovascular hypertension (to determine whether there is stenosis or obstruction) [6–12].

Detection of accessory renal arteries can be performed with angiographic studies [13, 14]. Recently MR angiography (MRA) and CT angiography (CTA) have been used for this purpose [11, 12, 15–24]. In particular it was shown that by optimizing the technical parameters it is possible to obtain excellent results with CTA [25, 26]. The main limitation of CT axial slices with respect to the direct coronal acquisition possible with MRA, is the precise evaluation of the distance of the accessory renal arteries from the main renal artery. This information can only be obtained in three-dimensional (3D) space by using multiplanar reconstructions or 3D models of the vessels, such as the maximum intensity projection (MIP) and shaded surface display (SSD).

Another possibility for displaying the aortic lumen is the internal surface rendering obtained with virtual vascular endoscopy (VVE) [27–34]. This technique reproduces a model of the internal walls with light and shade, visualized through a conic field of view simulating that of fiberoptic endoscopy systems. This perspective has been applied to the visualization of the inside of the aorta and its main branches, but has not been focused to evaluate its diagnostic accuracy for detecting accessory renal arteries. Therefore, the aim of

Correspondence to: E. Neri, M.D.

our study was to evaluate the diagnostic accuracy of VVE in the detection of accessory renal arteries.

Materials and Methods

We retrospectively reviewed the spiral CT (HiSpeed Advantage; GEMS, Milwaukee, WI, USA) data sets of 67 patients imaged for the study of the renal arteries, and affected by renovascular hypertension. All patients (29 male and 38 female; age range 17–72 years, mean age 53 years) were also evaluated with intraarterial digital subtraction angiography (DSA) (Multistar; Siemens, Erlangen, Germany).

DSA

DSA was performed using a 5 Fr pigtail catheter with transfemoral approach using the Seldinger technique. Contrast medium (Visipaque 370, Nycomed, Oslo, Norway) was injected at a flow rate of 12 ml/sec to a total volume of 24–30 ml, to perform flush aortography. Left anterior oblique projections were obtained, and if necessary right anterior and frontal views were added for optimal detection of the renal arteries. Flush aortography was considered the reference standard for accessory renal artery detection.

CTA

A single breath-hold scan of the tract including superior mesenteric and renal arteries was performed with the following parameters: tube rotation 1 sec, beam collimation 3 mm, pitch ratio 1 (3 mm/sec table incremental speed), tube current 120 kVp–280 mA, field of view (FOV) 30–35 cm. Acquisition time was 25–30 sec, and the total scanning length was 75–90 mm.

A volume of 150 ml of nonionic contrast (300 mgI/ml, Omnipaque 300, Nycomed) was administered with a power injector (MCT/MCT Plus, MEDRAD, Indianola, PA, USA) via the antecubital vein, at a flow rate of 3–4 ml/sec. To select the scan delay, the circulation time was determined with a dynamic scanning test through a semiautomatic bolus tracking program. No oral contrast agent was administered to avoid artifacts in the 3D model.

Images were reconstructed with a 180° linear interpolation algorithm. The CTA data set that included the renal arteries was reconstructed with 1-mm interslice interval. Spatial resolution of axial slices was 512×512.

Image Processing

All CTA data sets were processed with the Navigator software (GE, Milwaukee, WI, USA), running on a SunSparc 20 (Sun Microsystems, Mountain View, CA, USA) workstation. Navigator allowed the display of internal views of surface-rendered vessels. To generate internal views a preliminary segmentation of the data set was performed by means of a thresholding technique. After selection of the voxels representing the contrast medium inside the aorta, the internal surface was created with the "marching cube" algorithm. In this approach the boundary voxels of the volume were transformed into a smooth surface of triangles or patches [35].

Interaction with the images was by the "pick-a-point" (pp) function, that allowed a point in the endoscopic view to be selected and the corresponding axial, sagittal, and coronal views crossing through this point (VVE-pp) to be obtained in real time. In this way it was possible to verify each finding displayed on the VVE images by checking the other views.

MIP images were always obtained in the coronal (oblique) and axial (oblique) planes by creating subvolume reformations (Figs. 1, 2). The axial-oblique and coronal-oblique subvolume reformations were evaluated together, trying to keep the width of the slab as thin as possible, to enhance the visibility of even small vessels. No editing of skeletal structures was used, to avoid increasing the processing time.

Image Analysis

Two experienced radiologists (C.V., C.B.) independently evaluated on monitor the CT axial images and assessed them for the presence and number of accessory renal arteries. Subsequently they interactively performed MIP on the data sets, making their assessment. As a third step they were required to navigate through a pre-reconstructed VVE data set of the aorta (at the level of the renal arteries) and asked to make their assessment directly and by using the pp function (VVE-pp). To avoid the results of one display technique being influenced by the results of the others, the data sets were presented in each of the three subsequent assessments in random order and patient data were masked.

The final decision on the presence of accessory renal arteries was reached on the basis of a consensus between the observers. In the case of disagreement a tiebreaker radiologist (D.C.) was introduced.

The DSA images were reviewed by an independent observer (R.C.) whose assessment was taken as the gold standard of the study.

Statistical Analysis

True positives were defined as cases in which the display technique (axial, MIP, VVE, VVE-pp) correctly detected accessory renal arteries, as demonstrated at DSA. Accordingly, false positives were defined as cases in which the detection of accessory renal arteries was not confirmed by DSA; false negatives were the cases in which the considered display techniques were unable to detect accessory renal arteries shown at DSA; and true negatives were the cases in which accessory renal arteries were not detectable at either spiral CT or DSA. Sensitivity, specificity, positive predictive values, and negative predictive values were calculated for axial images, MIP, VVE, and VVE-pp.

The results of spiral CT imaging techniques, in terms of sensitivity and specificity, were compared with DSA by the χ^2 test. Statistical analysis was performed with StatView software (Abacus Concepts, Berkeley, CA, USA). A p value of less than 0.05 was considered to indicate a statistically significant difference.

Results

DSA identified the presence of 20 accessory renal arteries in 16 of 67 patients (23%). In four patients the accessory renal arteries were bilateral, in 11 cases they arose from the right and in five cases from the left side of the aorta.

Accessory renal arteries were found in 63% of cases on VVE, and in 88% of cases on axial images, MIP, and

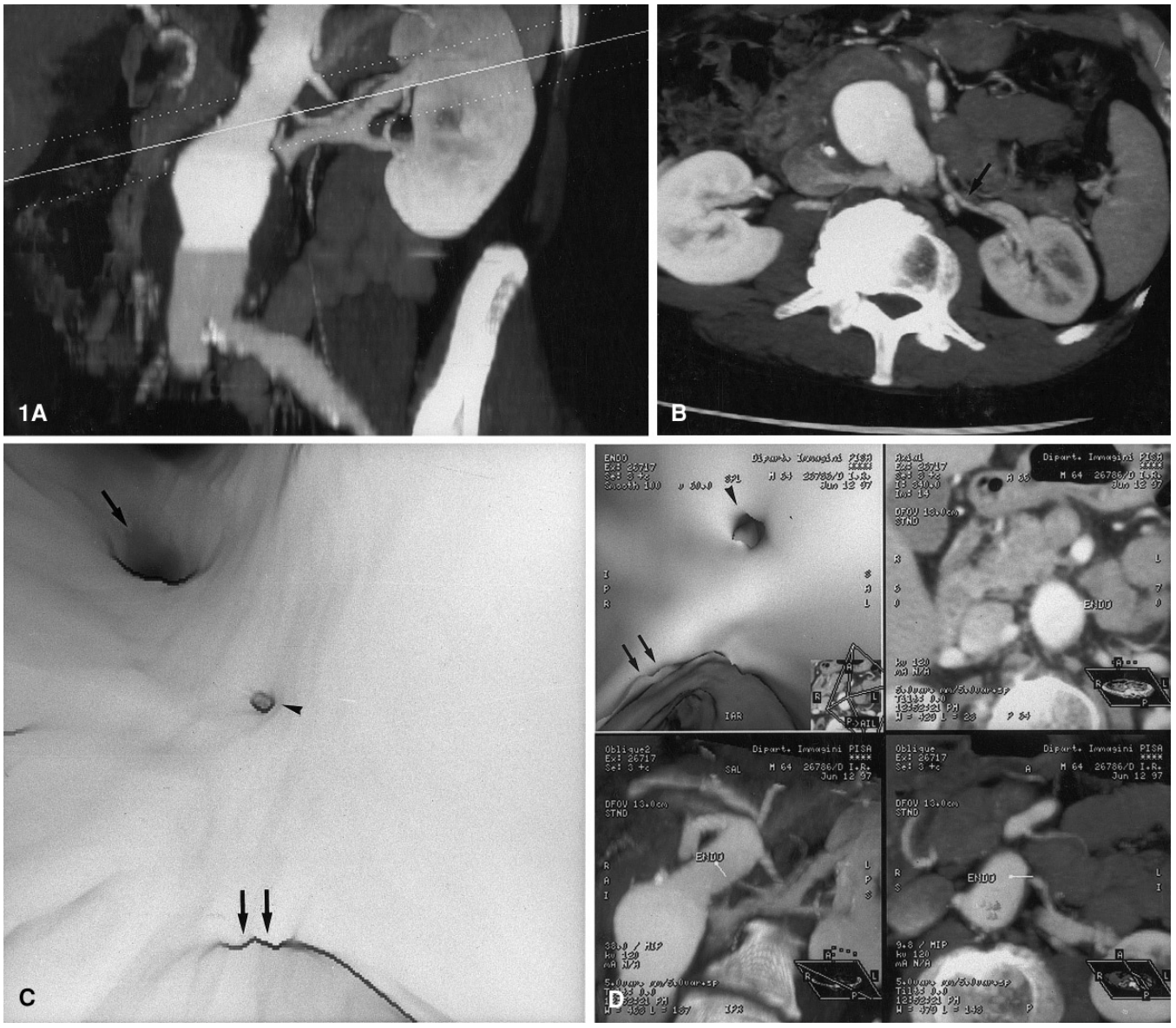

Fig. 1. Left accessory renal artery arising below the main renal artery in a patient with infrarenal abdominal aortic aneurysm. **A** Maximum intensity projection (MIP) of the aorta, obtained from a coronal subvolume reformation, which demonstrates the presence of a left accessory renal artery. This image is used to create a further subvolume reformation with a thickness of 22.4 mm, in the axial-oblique plane. **B** The resulting MIP shows the left accessory renal artery from the ostium to the renal hilum (arrow). **C** The endoscopic view, created from inside the lumen of the aorta looking toward the main (arrow) and accessory (arrowhead) renal arteries, reveals at a caudal level the neck of the aneurysm (double arrow). **D** If the screen is divided into four quadrants, and the pick-a-point function is used on the VVE-pp (upper left corner) to indicate the ostium of the accessory renal artery (arrowhead), above the neck of the aneurysm (double arrow), the axial image in the upper right corner, the MIP (coronal subvolume reformation) in the lower left corner, and the MIP (axial subvolume reformation) in the lower right corner demonstrate the ostium also.

VVE-pp. All results in terms of sensitivity, specificity, and positive and negative predictive values are shown in Table 1.

The best display techniques for detection of accessory renal arteries were VVE-pp and MIP, which did not show any statistically significant difference with respect to DSA (chi-square = 3.306, $p = 0.35$).

Discussion

VVE was the display technique with the highest number of false negatives (6 cases) and false positives (6 cases), and lowest negative (88%) and positive (62%) predictive values. False positives were represented by: two ostial stenoses of

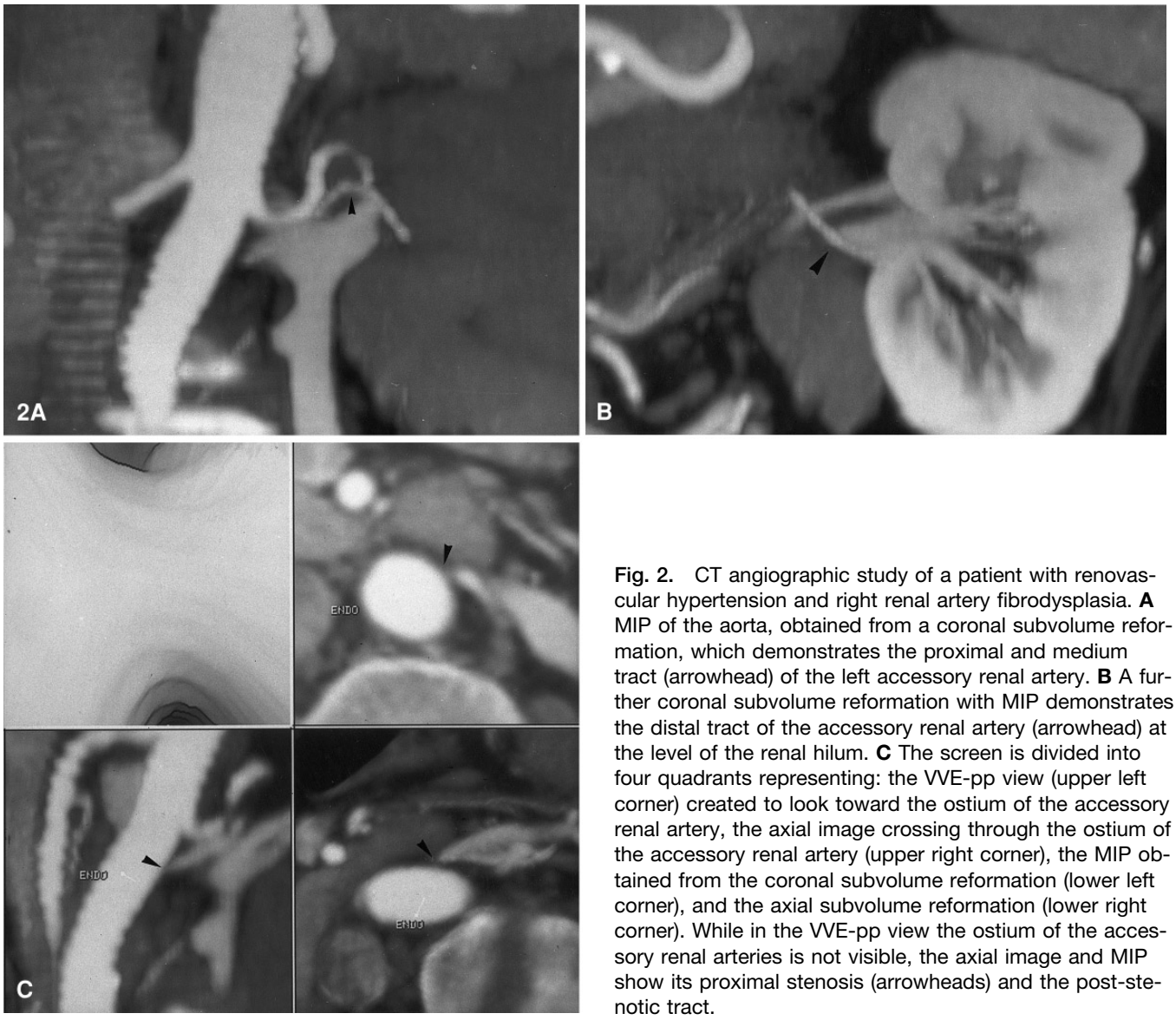

Fig. 2. CT angiographic study of a patient with renovascular hypertension and right renal artery fibrodysplasia. **A** MIP of the aorta, obtained from a coronal subvolume reformation, which demonstrates the proximal and medium tract (arrowhead) of the left accessory renal artery. **B** A further coronal subvolume reformation with MIP demonstrates the distal tract of the accessory renal artery (arrowhead) at the level of the renal hilum. **C** The screen is divided into four quadrants representing: the VVE-pp view (upper left corner) created to look toward the ostium of the accessory renal artery, the axial image crossing through the ostium of the accessory renal artery (upper right corner), the MIP obtained from the coronal subvolume reformation (lower left corner), and the axial subvolume reformation (lower right corner). While in the VVE-pp view the ostium of the accessory renal arteries is not visible, the axial image and MIP show its proximal stenosis (arrowheads) and the post-stenotic tract.

Table 1. Sensitivity, specificity, positive predictive value (PPV), negative predictive value (NPV), and statistical difference with respect to angiography of the imaging techniques

Display technique	False positives	True negatives	False negatives	True positives	Sensitivity (%)	Specificity (%)	PPV (%)	NPV (%)	Statistical difference with respect to DSA
Axial	3	48	2	14	88	94	82	96	NS
MIP	1	50	2	14	88	98	93	96	NS
VVE	6	45	6	10	63	88	62	88	$p < 0.05$
VVE-pp	1	50	2	14	88	98	93	96	NS
DSA	0	51	0	16	100	100	100	100	

NS = not statistically significant ($p > 0.05$); MIP = maximum intensity projection; VVE = virtual vascular endoscopy; pp = pick-a-point function; DSA = digital subtraction angiography.

the main renal arteries, interpreted as ostia of accessory renal arteries (in these cases axial images, MIP, and VVE-pp were able to correct the mistake); two adrenal artery ostia and one lumbar artery ostium located close to the main renal artery (axial images were falsely positive as well, while VVE-pp and MIP showed the absence of accessory renal arteries); and one case of incorrect segmentation of the data set, which caused the appearance of a "hole" through the wall of the aorta that simulated the ostium (true negative in the other display technique). Since we defined false positive results as

the cases not confirmed by DSA, accordingly these could have been accessory arteries missed by DSA. Indeed in some cases projection effects may obscure the accessory renal arteries and lead to a misinterpretation in angiography.

False negatives of VVE were represented by: two ostial stenoses of the accessory renal arteries (Fig. 2); one case of calcified plaque obscuring the ostium; and three cases of incorrect segmentation that prevented representation of the ostium. In all cases the accessory renal arteries were correctly demonstrated with the other display techniques.

The main limitation of VVE was represented by the presence of segmentation artifacts, which affected both false positive and false negative results [36, 37]. The "hole" through the aorta was misinterpreted as an ostium, and by contrast three real ostia of accessory renal arteries were masked since the density range selected for segmentation did not include them. Further limitations of VVE were represented by the lack of anatomic orientation, the presence of calcified plaques over the ostia and ostial stenosis of the renal arteries. All these limitations depend on the lack of transparency, typical of VVE based on surface rendering, that does not allow visualization from inside the aorta of the outer tract of the accessory renal arteries. The assessment of the ostium from inside the lumen is restricted to the evaluation of its morphology, position, and patency. The ostium and the lumen of the main renal artery and of the accessory renal artery can be visualized with VVE if the contrast enhancement is adequate, if the image includes all the voxels belonging to the artery, if there is no stenosis, and if there are no calcified plaques obscuring the ostium.

In our experience, the solution to some of these issues was obtained by using the pp function. VVE-pp increased sensitivity and specificity since it is based on integration with other display techniques. Axial images and MIP were exploited as added perspectives that allowed the outer part of the accessory renal arteries to be visualized from inside the aorta. Despite this, VVE-pp had two false negative cases that corresponded to patients who were also incorrectly evaluated by axial images and VVE, but in whom MIP was able to detect the accessory renal arteries. In these patients the left accessory renal arteries had ostial stenosis that prevented the visualization of the ostium from inside the lumen of the aorta (Fig. 2). The missed visualization of ostia did not alert the observers to investigate further the possible presence of accessory renal arteries. A false positive diagnosis of accessory renal artery made by VVE-pp occurred in a patient in whom the right adrenal artery arose very close to the main right renal artery and was located just above its ostium. This case was falsely positive with MIP and axial images as well.

In the case of MIP, both observers misdiagnosed two accessory renal arteries as adrenal arteries (false negative cases); the same mistake was made with axial slices also. A retrospective evaluation of the same cases, with knowledge of the DSA patterns, allowed the MIP to be performed correctly and visualization of the vessels to be obtained. After this evaluation, the sensitivity of MIP increased to 100%. By contrast, axial images were not able to depict the distal portion of the accessory renal arteries even in a retrospective evaluation.

If the main advantage of MIP was to create multiple oblique planes along the artery path that allowed it to be followed to the renal hilum (Figs. 1, 2), in the case of axial images this appears to be the major limitation. Axial slices had the same two false positive cases as MIP, with two further false positive cases represented by lumbar arteries incorrectly evaluated on the slices above or below the origin.

The initial purpose of our study was to evaluate the sensitivity and specificity of VVE in the detection of accessory renal arteries. Analysis of the observations allows us to conclude that VVE alone has a poor accuracy, and does not substantially improve the sensitivity and specificity of CTA. By contrast, the results in terms of sensitivity, specificity, negative predictive value, and positive predictive value of MIP demonstrated that this technique was the most reliable for the detection of accessory renal arteries. In fact, it allowed detection of the accessory renal arteries without integration with other imaging techniques.

The usefulness of VVE is significantly enhanced if it is integrated with the pp function. VVE-pp overcame the limitation of surface rendering, allowing evaluation of the accessory renal arteries from outside the lumen as well. In our opinion VVE, if integrated with the pp function, can give 3D information on the relationships between the accessory renal arteries and the main renal artery, accessory renal arteries and the neck of aneurysms, and accessory renal arteries and calcified plaques (Fig. 1).

It is still too early to conclude that VVE-pp may be able to replace axial slices and thin-slab MIP in the evaluation of accessory renal arteries. However, our results suggest that this technique, allowing direct display of the accessory ostium, may be useful. We believe that the value of VVE-pp will be further enhanced when volume-rendered reconstructions are available in addition to surface-rendered ones.

References

1. Gray H (1995) Gray's Anatomy. Churchill Livingstone, New York, pp 1826–1827
2. Poisel S, Spongler HP (1969) On aberrant and accessory renal arteries in kidneys of typical position. Anat Anz 124:244–259
3. Armstrong BG, Hunt TH, Price CW, Resnick MI (1979) Common origin of inferior mesenteric and accessory renal artery. Urology 14: 298–299
4. Nathan H, Glezer I (1984) Right and left accessory renal arteries arising from a common trunk associated with unrotated kidneys. J Urol 132: 7–9
5. Goscicka D, Szpinda M, Kochan J (1996) Accessory renal arteries in human fetuses. Anat Anz 178:559–563
6. Lingos J, Docolomansk A, Blazicek P, Novotn J, Krcmèry S, Rozhold Z, Gergel C (1972) Accessory renal arteries and their significance in the pathogenesis of systemic hypertension. Bratisl Lek Listy 58:188–198
7. Tsakadze LO, Solovev VA (1975) Multiple renal arteries and their importance in surgery of aneurysm of the abdominal aorta. Vestn Khir 114:53–58
8. Connelly TL, McKinnon W, Smith RB III, Perdue GD (1980) Abdominal aortic surgery and horseshoe kidney. Arch Surg 115:1459–1463
9. De Virgilio C, Gloviczki P (1996) Aortic reconstruction in patients with horseshoe or ectopic kidney. Semin Vasc Surg 9:245–252

10. Oesterwitz H, Strobelt V, Scholz D, Mebel M (1985) Extracorporeal microsurgical repair of injured multiple donor kidney arteries prior to cadaveric allotransplantation. Eur Urol 11:100–105
11. Debatin JF, Sostman HD, Knelson M, Argabright M, Spritzer CE (1993) Renal magnetic resonance angiography in the preoperative detection of supernumerary renal arteries in potential kidney donors. Invest Radiol 28:882–889
12. Gourlay WA, Yucel EK, Hakaim AG, O'Meara YM, Mesler DE, Kerr K, Cho SI (1995) Magnetic resonance angiography in the evaluation of living-related renal donors. Transplantation 60:1363–1366
13. Fontaine R, Kieny R, Jurascheck F, Perezcay C (1965) Angiographic study of the accessory renal arteries (superior and inferior polar arteries independent of the normal renal arteries) and their pathological significance. Lyon Chir 61:685–702
14. Danek Z (1974) Accessory renal arteries in aortonephrography. Pol Przegl Radiol 38:31–38
15. Galanski M, Prokop M, Chavan A, Schaefer CM, Jandeleit K, Nischelsky JE (1993) Renal artery stenoses: Spiral CT angiography. Radiology 189:185–192
16. Rubin GD, Dake MD, Napel S, Jeffrey RB, McDonnell CH, Sommer FG, Wexler L, Williams DM (1994) Spiral CT of renal artery stenosis: Comparison of three-dimensional rendering techniques. Radiology 190: 181–189
17. Rubin GD, Walker PJ, Dake MD, Napel S, Jeffrey RB, McDonnell CH, Mitchell RS, Miller DC (1993) Three-dimensional spiral computed tomographic angiography: An alternative imaging modality for the abdominal aorta and its branches. J Vasc Surg 18:656–664
18. Rubin GD, Alfrey EJ, Dake MD, Semba CP, Sommer FG, Kuo PC, Dafoe DC, Waskerwitz JA, Bloch DA, Jeffrey RB (1995) Assessment of living renal donors with spiral CT. Radiology 195:457–462
19. Platt JF, Ellis JH, Korobkin M, Reige KA, Konnak JW, Leichtman AB (1996) Potential renal donors: Comparison of conventional imaging with helical CT. Radiology 198:419–423
20. Rieker O, Duber C, Schmiedt W, Neufang A, Pitton M, Schweden F (1996) CT angiography versus intra-arterial DSA in abdominal aortic aneurysms. Rofo Fortschr Geb Rontgenstr Neuen Bildgeb Verfahr 165:17–23
21. Cikrit DF, Harris VJ, Hemmer CG, Kopecky KK, Dalsing MC, Hyre CE, Fischer JM, Lalka SG, Sawchuk AP (1996) Comparison of spiral CT scan and arteriography for evaluation of renal and visceral arteries. Ann Vasc Surg 10:109–116
22. Adachi H, Ino T, Mizuhara A, Yamaguchi A, Kobayashi Y, Nagai J (1994) Assessment of aortic disease using three-dimensional CT angiography. J Card Surg 9:673–678
23. Balm R, Eikelboom BC, van Leeuwen MS, Noordzij J (1994) Spiral CT-angiography of the aorta. Eur J Vasc Surg 8:544–551
24. Holland GA, Dougherty L, Carpenter JP, Golden MA, Gilfeather M, Slossman F, Schnall MD, Axel L (1996) Breath-hold ultrafast three-dimensional gadolinium-enhanced MR angiography of the aorta and the renal and other visceral abdominal arteries. AJR 166:971–981
25. Diederichs CG, Keating DP, Glatting G, Oestmann JW (1996) Blurring of vessels in spiral CT angiography: Effects of collimation width, pitch, viewing plane, and windowing in maximum intensity projection. J Comput Assist Tomogr 20:965–974
26. Brink JA, Lim JT, Wang G, Heiken JP, Deyoe LA, Vannier MW (1995) Technical optimization of spiral CT for depiction of renal artery stenosis: In vitro analysis. Radiology 194:157–164
27. Rubin GD, Beaulieu CF, Argiro V, Ringl H, Norbash AM, Feller JF, Dake MD, Jeffrey RB, Napel S (1996) Perspective volume rendering of CT and MR images: Applications for endoscopic imaging. Radiology 199:321–330
28. Davis CP, Ladd ME, Romanowski BJ, Wildermuth S, Knoplioch JF, Debatin JF (1996) Human aorta: Preliminary results with virtual endoscopy based on three-dimensional MR imaging data sets. Radiology 199:37–40
29. Kimura F, Shen Y, Date S, Mochizuki T (1996) Thoracic aortic aneurysm and aortic dissection: New endoscopic mode for three-dimensional CT display of the aorta. Radiology 198:573–578
30. Ladd ME, Gohde SC, Steiner P, Pfammatter T, McKinnon GC, Debatin JF (1996) Virtual MR angioscopy of the pulmonary artery tree. J Comput Assist Tomogr 20:782–785
31. Hayashi H, Kobayashi H, Kumazaki T (1996) Three-dimensional measurement of vascular lesions with virtual CT endoscopy "cruising eye view" method. Nippon Igaku Hoshasen Gakkai Zasshi 56:880–882
32. Hayashi H, Kobayashi H, Kumazaki T, Goto Y (1996) Virtual CT endoscopy "cruising eye view": Development and clinical applications. Nippon Igaku Hoshasen Gakkai Zasshi 56:135–136
33. Igel BJ, Durham NC, McDermott VG, Nelson RC (1996) Abdominal aortic aneurysms from the inside out: Applications and limitations of virtual angioscopy. Radiology 201(P):467
34. Bartolozzi C, Neri E, Caramella D (1997) CT in vascular pathologies. Eur Radiol 8:679–684
35. Lorensen WE, Cline H (1987) Marching cubes: A high resolution 3D surface construction algorithm. Comput Graphics 21:163–169
36. Neri E, Caramella D, Falaschi F, Sbragia P, Vignali C, Bartolozzi C (1997) Virtual endoscopy of the aorta: Segmentation artifacts with perspective surface rendering of spiral CT data sets. Radiology 205(P): 262
37. Neri E, Caramella D, Falaschi F, Sbragia P, Laiolo E, Bartolozzi C (1997) Virtual endoscopy of the aorta: Role of segmentation artifacts in the visualization of detected findings. Radiology 205(P):623